Examination of Transport Theory of Arbitrary Order in Velocity Variance by MRI

N. C. Irwin and R. A. Greenkorn
School of Chemical Engineering, Purdue University, West Lafayette, IN 47907

S. A. Altobelli
New Mexico Resonance, Albuquerque, NM 87108

J. H. Cushman
Center for Applied Mathematics, Purdue University, West Lafayette, IN 47907

Subsurface heterogeneity makes the accurate modeling of flow in natural porous systems challenging. Because of the uncertainty associated with flow and transport in these systems, researchers have adopted a stochastic approach to modeling. Common to this approach is the assumption that triplet correlation terms involving fluctuating velocities and fluctuating concentration are insignificant relative to terms containing doublet cross correlations. This assumption is considered valid for a log-hydraulic conductivity variance σ_f^2 on the order of one (Dagan, 1985, 1993; Tompson and Gelhar, 1990; Deng and Cushman, 1995). However, recent numerical (Hassan, 1995) and experimental (Irwin et al., 1998) studies suggest that the upper limit on σ_f^2 may be less than unity. Thus, neglecting triplet correlation terms may have significant implications for the modeling of large-scale flow and transport processes in natural systems.

Cushman and Hu (1997) report an alternate approach to the solution of the Eulerian transport problem. A recursive perturbation solution is developed for a conservative solute in a random conductivity field. The stochastic concentration is given to arbitrary order in σ_v. The new approach appears to eliminate the need to make assumptions about the significance of triplet correlation terms involving fluctuating velocities and fluctuating concentration. The accuracy of the closure scheme may be quantified as it is solely a function of higher-order velocity correlation functions. While the accuracy of this new approach may be explored numerically, its applicability may also be examined experimentally. Since the closure scheme depends solely on velocity correlation functions, it is easily investigated using MRI flow measurement techniques. Preliminary results are reported to illustrate how MRI techniques can be applied to examine the validity of the closure scheme.

Correspondence concerning this article should be addressed to R. A. Greenkorn.

Experimental Studies

MRI techniques were applied to make three-dimensional (3-D) images of the velocity field in an experimental model. The model was constructed by packing a Lucite column, 3.18 cm in diameter and 61.0 cm in length, with a distribution of unconsolidated spherical glass beads. The beads had a U.S. Sieve Series size distribution of 20–30 mesh (590–840 μm) and a mean diameter of 700 μm. The measured porosity and permeability were 0.340 and 227 darcy, respectively. The average pore size was on the order of 200 μm. Longitudinal dispersion coefficients were measured along the length of the experimental model using an electrochemical measurement technique (Irwin et al., 1996). The longitudinal dispersion was found to be constant along the length of the model with an average dispersivity of 0.461 cm. A constant dispersion coefficient is consistent with Fickian behavior; thus, the macroscale mixing in this model may be described by an average dispersion coefficient. Since the model can be accurately represented by average properties, it is referred to as "homogeneous."

The imaging experiments were performed on a Tecmag LIBRA imager interfaced to a 31 cm horizontal bore superconducting magnet at a field of 1.89 T. The Larmor frequency for ^{1}H at this field was 80.34 MHz. The magnet contained actively shielded gradient coils and a high-pass bird cage radio frequency (rf) probe. A modified stimulated echo imaging sequence (Waggoner and Fukushima, 1996), shown in Figure 1, was used to make 3-D images of the x-, y- and z-components of the velocity field in the homogeneous model. During velocity imaging, spatial discrimination is achieved by applying magnetic field gradients G_r and G_p along orthogonal axes. The read-out gradient G_r is applied along z to impart a frequency proportional to the z-coordinate of the corresponding voxel. Phase-encoding gradients G_p are applied along x and y to modulate the signal phase by an amount proportional to

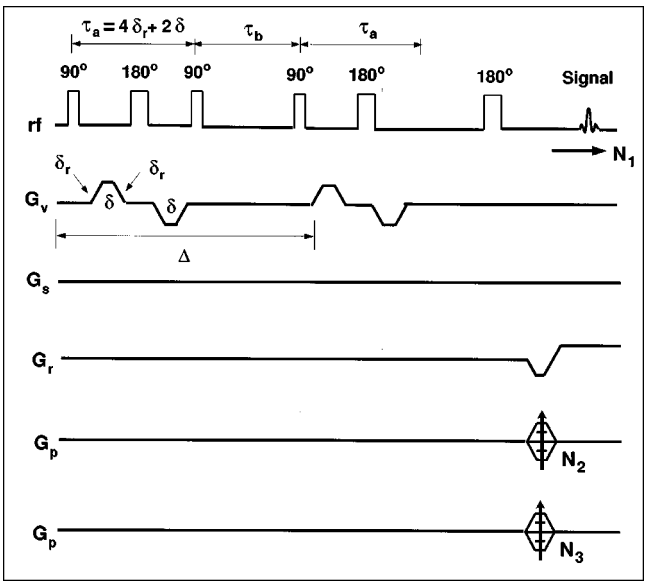

Figure 1. 3-D stimulated echo velocity imaging sequence.

the *x*- and *y*-coordinates of the voxel from which it is derived. Velocity encoding is achieved by applying an additional gradient G_v along *x*, *y*, or *z*, depending on which velocity component is desired. To produce a 3-D image, the basic sequence is repeated with 32 phase encodes (N_2) along *x* and 16 phase encodes (N_3) along *y*. During each of the repetitions, 64 points (N_1) are digitized during the period marked ''signal'' in Figure 1. The final image is then obtained by a 3-D Fourier transform of the N_1 by N_2 by N_3 complex array.

Results and Discussion

3-D images were made of each of the velocity components in a 10 cm section of the homogeneous model, 30 cm from the inlet of the model, at an average linear velocity of 0.05 cm/s. The resolution of each 3-D image is 3.2 mm in the *x* direction, 3.2 mm in the *y* direction, and 2.8 mm in the *z* direction. Thus, there are approximately 40 beads in each 29 mm^3 voxel. It has been argued that resolution below the pore scale is necessary in order to obtain reliable data (Nesbitt et al., 1992). For these experiments, an average measurement over several pores was considered appropriate since the theoretical model is based on a Darcy-scale or superficial velocity.

Each velocity experiment requires that two complex spin density images be recorded. With no flow, a static image S_0 is taken with negligible first moment. While the fluid is moving, a flowing image M_0 is obtained using the same first moment. A phase image is computed from the complex spin density images according to

$$\phi = \arctan\left(\frac{\Re(M_0/S_0)}{\Im(M_0/S_0)}\right) \tag{1}$$

where $\Im$ and $\Re$ represent the imaginary and real part of the complex image data, respectively. The resulting phase image is converted to a velocity image via the velocity sensitivity *u* of the measured phase of spin precession to flow velocity

$$V = u\phi \tag{2}$$

The magnetization phase shift due to displacement ϕ for the stimulated echo sequence shown in Figure 1 is

$$\phi = \gamma V_0 \int G_v(t)\, t\, dt \tag{3}$$

where V_0 is the average velocity of the fluid in the voxel, *t* is time, and $G_v(t)$ is the time-dependent magnetic field gradient that gives rise to velocity sensitivity. Performing the integration of Eq. 3 yields

$$\phi = 2\gamma g V_0 \Delta(\delta + \delta_r) \tag{4}$$

where $g = G_2 - G_1$ is the difference in magnitude of the velocity encoding gradients in successive measurements and

$$\Delta = \tau_a + \tau_b \tag{5}$$

$$\tau_a = 4\delta_r + 2\delta \tag{6}$$

The gradient pulse parameters Δ, δ, δ_r, τ_a and τ_b are defined in Figure 1. The greatest sensitivity to flow can be achieved by maximizing ϕ/V_0 which can be achieved, in turn, by maximizing *g*, Δ, and/or δ. Thus, the velocity sensitivity *u* is determined according to

$$u = \phi/V_0 = 2\gamma g \Delta(\delta + \delta_r) \tag{7}$$

The gradient pulse parameters and velocity sensitivities computed according to Eq. 7 for the velocity imaging experiments are presented in Table 1.

Two- and three-point velocity correlation functions were estimated from the velocity data according to (Wei, 1990)

$$R(u_1) = \frac{1}{N}\sum_{i=1}^{N-u_1}\left(W_i - \overline{W}\right)\left(W_{i+u_1} - \overline{W}\right) \tag{8}$$

and

$$R(u_1,u_2) = \frac{1}{N}\sum_{i=1}^{N-u_1-u_2}\left(W_i - \overline{W}\right)\left(W_{i+u_1} - \overline{W}\right)\left(W_{i+u_2} - \overline{W}\right) \tag{9}$$

Table 1. Gradient Pulse Parameters and Computed Velocity Sensitivities for Velocity Images at 0.05 cm/s using the Stimulated Echo Sequence in Figure 1

Component	δ (ms)	δ_r (ms)	τ_b (ms)	Δ (ms)	γg (Hz/cm)	u (rad/cm/s)
x	5	0.5	40	52	$2\pi(400)(8.7)$	12.5
y	5	0.5	40	52	$2\pi(400)(7.8)$	11.2
z	5	0.5	40	52	$2\pi(400)(9.3)$	13.4

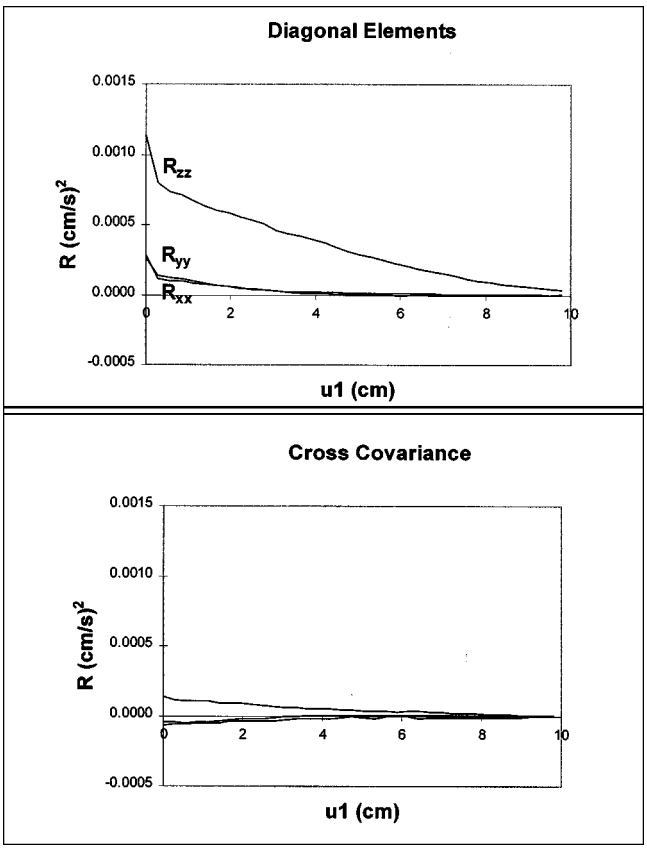

Figure 2. Two-point correlation functions determined from the 3-D velocity images in the homogeneous model.

Values computed according to Eq. 8.

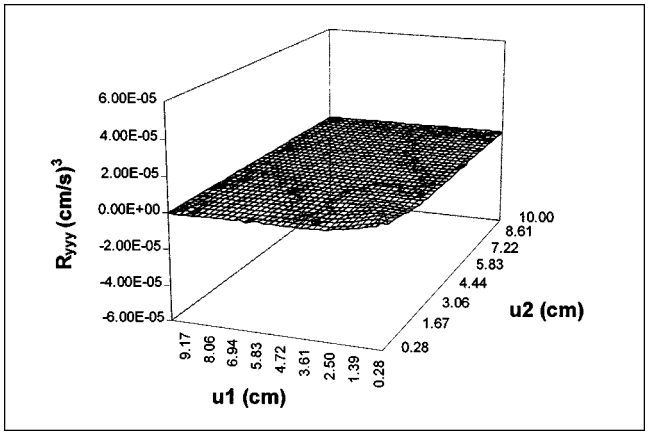

Figure 4. Three-point correlation function R_{yyy} determined from the 3-D velocity image in the homogeneous model.

Values computed according to Eq. 9.

where W is the mean of the process, u_1 and u_2 are the lags at which correlation is estimated, i is the location at which W has been measured, and N is the total number of observations. It should be noted that the correlation functions determined from the imaging data were computed with a sample size of $N = 36$. Box (1976) suggests that useful estimates of the covariance can only be made if the number of data points N is roughly 50 or more. Thus, any conclusions drawn from these preliminary results may require further investigation. A set of 3-D images made along the length of the model would provide a more extensive data set for the evaluation of the closure scheme.

The two-point correlation functions are illustrated in Figure 2. The diagonal elements of three-point correlations R_{xxx}, R_{yyy}, and R_{zzz} are shown in Figures 3–5. An examination of the relative magnitude of the two- and three-point correlations suggests that the three-point correlations are quite small relative to the two-point correlations. In fact, the data in Figures 3–5 suggest that the three-point correlations are essen-

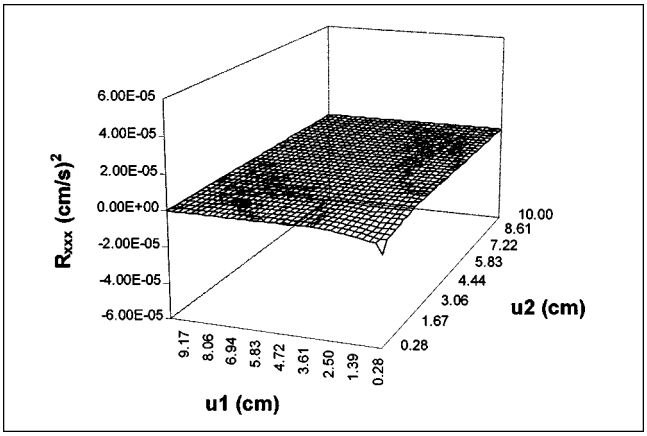

Figure 3. Three-point correlation function R_{xxx} determined from the 3-D velocity image in the homogeneous model.

Values computed according to Eq. 9.

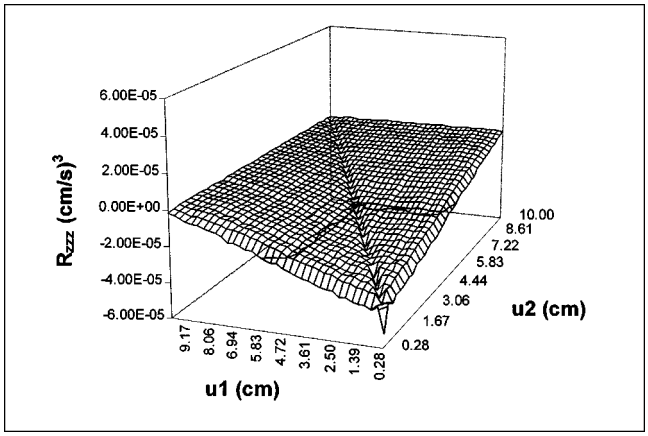

Figure 5. Three-point correlation function R_{zzz} determined from the 3-D velocity image in the homogeneous model.

Values computed according to Eq. 9.

tially zero. However, a closer look at the three-point correlations suggests that some structure may be evident in these terms. Although small, this structure may have an effect on mixing behavior. The comparison of two- and three-point correlations determined from a larger sample size ($N > 50$) would provide a more extensive data set for the examination of the relative magnitude of higher-order correlations. Nonetheless, these preliminary results demonstrate that MRI techniques can be easily applied to examine the accuracy of the closure scheme.

Conclusions

Experiments were performed to determine if velocity imaging techniques could be applied to evaluate the closure scheme of a recursive perturbation solution to the Eulerian transport problem. 3-D images were made of the velocity field in a homogeneous model to estimate the relative magnitude of two- and three-point velocity correlation functions. No definitive conclusions were drawn from the preliminary results since the data from a single image produced too small a sample size for the determination of reliable correlation functions. Nonetheless, these preliminary results demonstrate how MRI techniques can be applied to estimate velocity correlation functions for the evaluation of such closure schemes.

Notation

γ = gyromagnetic ratio
ϕ = magnetization phase shift due to displacement
σ_v^N = velocity variance of order N

Literature Cited

Box, G. E. P., *Time Series Analysis: Forecasting and Control*, Holden-Day, Boca Raton, FL (1976).

Cushman, J. H., and B. X. Hu, "Solution to the Stochastic Transport Problem of $O(\sigma_v^N)$ for Conservative Solutes," *Stoch. Hydrol. Hydraulics*, **11**, 297 (1997).

Dagan, G., "A Note on Higher-Order Corrections to the Head Covariances in Steady Aquifer Flow," *Water Res. Res.*, **21**, 573 (1985).

Dagan, G., "Higher-Order Correction of Effective Permeability of Heterogeneous Isotropic Formations of Lognormal Conductivity Distribution," *Transp. Porous Media*, **12**, 279 (1993).

Deng, F.-W., and J. H. Cushman, "On Higher-Order Corrections to the Flow Velocity Covariance Tensor," *Water Res. Res.*, **31**, 1659 (1995).

Hassan, A. E., "Monte Carlo Simulations of Flow and Transport in Heterogeneous Porous Media: an Evaluation of First- and Second-Order Theories and the Importance of Porosity Variability," PhD Thesis, Purdue University (1995).

Irwin, N. C., M. M. Botz, and R. A. Greenkorn, "Experimental Investigation of Characteristic Length Scale in Periodic Heterogeneous Porous Media," *Transp. Porous Media*, **25**, 235 (1996).

Irwin, N. C., S. A. Altobelli, J. H. Cushman, and R. A. Greenkorn, "Examination of Stochastic Perturbation Theory by Magnetic Resonance Imaging in Aperiodic Heterogeneous Porous Media," *Water Res. Res.*, in press (1999).

Nesbitt, G. J., T. W. Fens, J. S. van den Brink, and N. Roberts, "Evaluation of Fluid Displacement in Porous Media Using NMR Microscopy," in *Magnetic Resonance Microscopy: Methods and Application in Materials Science, Agriculture, and Biomedecine*, B. Blumich and W. Kuhn, eds., VCH Publishers, New York, p. 286 (1992).

Tompson, A. F. B., and L. W. Gelhar, "Numerical Simulation of Solute Transport in Three-Dimensional, Randomly Heterogeneous Porous Media," *Water Res. Res.*, **26**, 2541 (1990).

Waggoner, R. A., and E. Fukushima, "Velocity Distribution of Slow Fluid Flows in Bentheimer Sandstone: an NMRI and Propagator Study," *Magn. Reson. Imaging*, **14**, 1085 (1996).

Wei, W. W. S., *Time Series Analysis: Univariate and Multivariate Methods*, Addison-Wesley, Reading, MA (1990).

Manuscript received Sept. 8, 1998, and revision received Mar. 29, 1999.